Journal of the Endocrine Society, 2023, **7**, 1–14
https://doi.org/10.1210/jendso/bvac143
Advance access publication 16 September 2022
Research Article

Effect of Inactivation of *Mst1* and *Mst2* in the Mouse Adrenal Cortex

Nour Abou Nader,[1] Étienne Blais,[1] Guillaume St-Jean,[1] Derek Boerboom,[1] Gustavo Zamberlam,[1] and Alexandre Boyer[1]

[1]Centre de Recherche en Reproduction et Fertilité, Faculté de Médecine Vétérinaire, Université de Montréal, Saint-Hyacinthe J2S 7C6, Canada

Correspondence: Dr Alexandre Boyer, Centre de Recherche en Reproduction et Fertilité, Faculté de Médecine Vétérinaire, Université de Montréal, 3200 rue Sicotte, St-Hyacinthe, QC J2S 7C6, Canada. Email: alexandre.boyer.1@umontreal.ca.

Abstract

Recent conditional knockout of core components of the Hippo signaling pathway in the adrenal gland of mice has demonstrated that this pathway must be tightly regulated to ensure proper development and maintenance of the adrenal cortex. We report herein that the most upstream kinases of the pathway, the mammalian STE20-like protein kinases 1 and 2 (MST1and MST2, respectively), are expressed in the mouse adrenal cortex with MST2 expression being restricted to the zona glomerulosa (zG). To further explore the role of Hippo signaling in adrenocortical cells, we conditionally deleted *Mst1/2* in steroidogenic cells using an Nr5a1-cre strain (*Mst1*$^{flox/flox}$; *Mst2*$^{flox/flox}$; *Nr5a1*-cre). Our results show that the loss of MST1/2 leads to the premature and progressive accumulation of subcapsular GATA4+, WT1+ adrenal gonadal primordium (AGP)-like progenitor cells starting at 2 months of age without affecting aldosterone and corticosterone secretion. To help us understand this phenotype, microarray analyses were performed on adrenal glands from 2-month-old mutant and control mice. Gene expression analyses revealed that loss of *Mst1/2* leads to the overexpression of known downstream target genes (*Ajuba*, *Aqp1*, *Fn1*, *Ibsp*, *Igf1*, *Igfbp2*, *Mmp2*, *Thbs1*) of the main effector of Hippo signaling, YAP; and underexpression of genes (*Agtr1b*, *Ecgr4*, *Hsd3b6*, *Nr0b1*, *Tesc*, *Vsnl1*) that are normally specifically expressed in the zG or overexpressed in the zG compared to the zona fasciculata (zF). Together, these results suggest that MST1/2 regulates Hippo signaling activity in the adrenal cortex and that these two kinases are also involved in the fine tuning of zG cell function or differentiation.

Key Words: MST1, MST2, adrenocortical cells, adrenal gland, transgenic mouse

Abbreviations: AGP, adrenal gonadal primordium; AGTR1B, angiotensin receptor 1b; AQP1, aquaporin 1; CAS3, cleaved caspase-3; DAB2, Disabled 2, mitogen-responsive phosphoprotein; ECRG4, esophageal cancer related gene 4; FN1, fibronectin 1; FSH, follicle-stimulating hormone; GATA4, GATA binding protein 4; HSD3B6, hydroxy-delta-5-steroid dehydrogenase, 3 beta- and steroid delta-isomerase 6; IBSP, integrin-binding sialoprotein; IGF1, insulin-like growth factor 1; IGF2, insulin-like growth factor 2; IGFBP2, insulin-like growth factor binding protein 2; ITGA2, integrin alpha 2; LATS, large tumor suppressor homolog kinase; LH, luteinizing hormone; MMP2, matrix metallopeptidase 2; MST, mammalian STE20–like protein kinase; NR5A1, Nuclear receptor subfamily 5, group A, member 1; NR0B1, nuclear receptor subfamily 0, group B, member 1; PCR, polymerase chain reaction; PIANP, PILR alpha associated neural protein; PKA, protein kinase A; PTGS2, prostaglandin-endoperoxyde synthase 2; SHH, Sonic Hedgehog; STK, serine/threonine kinase; TAZ, transcriptional coactivator with PDZ-binding motif; TCF21, transcription factor 21; TESC, tescalcin; THBS1, thrombospondin 1; VSNL1, visilin like 1; WT1, Wilms tumor 1; YAP, Yes-associated protein; zF, zona fasciculata; zG, zona glomerulosa.

The adult adrenal gland is an endocrine organ essential to the regulation of bodily homeostasis. It is formed of concentric zones of steroidogenic cells that surround the chromaffin cells of the medulla. In mice, the adrenal cortex is subdivided into 2 concentric zones, each responsible for the production of a specific hormone, the outer zone, the zona glomerulosa (zG), synthesizes mineralocorticoids while the inner zone, the zona fasciculata (zF), produces glucocorticoids [1]. Throughout life, the replenishment of the adrenal cortex and the maintenance of zonation are crucial. In homeostatic conditions, maintenance of the definitive adrenal cortex mainly relies on proliferation of Sonic Hedgehog (SHH)–positive progenitor cells located within the zG in males [2, 3] while females rely on both the SHH-positive progenitor cells and the capsular GLI-Kruppel family member 1 (GLI1)–positive stem cells [2]. Progenitor cells further differentiate into steroidogenic zG cells, which in turn differentiate into zF cells through centripetal migration and zonal differentiation processes resulting from the antagonistic actions of the WNT/CTNNB1 and the protein kinase A (PKA) pathways [4–9]. Though SHH-WNT/CTNNB1-PKA are the most important pathways involved in the maintenance of the definitive cortex, additional pathways are also important for these processes.

Hippo is an evolutionarily conserved signaling pathway with essential roles in the development and homeostasis of many tissues [10, 11]. Core components of the Hippo signaling cascade include the mammalian STE20–like protein kinases 1 and 2 (MST1 and MST2, also known as serine/threonine kinase 3 and 4 [STK3, STK4]), the large tumor suppressor homolog kinases 1 and 2 (LATS1, LATS2) and 2 functionally redundant transcriptional coactivators, Yes-associated protein (YAP) and transcriptional coactivator with PDZ-binding motif (TAZ). In response to various intracellular and extracellular signals, MST1/2 are first phosphorylated and activated.

Received: 1 June 2022. **Editorial Decision:** 13 September 2022. **Corrected and Typeset:** 17 November 2022

Following their activation, MST1/2 phosphorylate and activate LATS1/2, which in turn phosphorylate YAP and TAZ, which cause their inactivation either by sequestration in the cytoplasm or by proteasome-mediated degradation. When the cascade is inactivated, YAP and TAZ accumulate in the nucleus and interact with transcriptional factors to regulate the transcription of genes involved in cell growth, apoptosis, and proliferation [12, 13].

Two studies using transgenic mice models have previously evaluated the role of Hippo signaling in the development and maintenance of the definitive adrenal cortex. It was first shown that concomitant loss of *Yap* and *Taz* in steroidogenic adrenocortical cells leads to the progressive degeneration of the adrenal cortex [14]. A subsequent study then showed that concomitant loss of *Lats1* and *Lats2* leads to the transdifferentiation of the adrenocortical cells of the definitive cortex into myofibroblast-like cells during embryonic development, resulting in adrenal failure and death by 3 weeks of age [15]. Taken together, these 2 studies suggest that Hippo signaling must be tightly regulated for the maintenance and development of the adrenal cortex. In this study, we decided to further delineate the role of the Hippo pathway in the adrenal gland. For this, we generated a mouse model in which *Mst1* and *Mst2*, the most upstream protein kinases of the Hippo pathway, were conditionally deleted in steroidogenic cells of the adrenal cortex (Nuclear receptor subfamily 5, group A, member 1 (NR5A1)–positive cells).

Material and Methods

Ethics

All animal procedures were approved by the Comité d'Éthique de l'Utilisation des Animaux of the Université de Montréal (protocol numbers Rech-1739 and Rech-1909) and conformed to the guidelines of the Canadian Council on Animal Care.

Transgenic Mouse Strains

Nr5a1-cre (FVB-Tg-Nr5a1Cre7Lowl/J, RRID:IMSR_JAX:012462 [16]) and $Mst1^{flox/flox}$;$Mst2^{flox/flox}$ ($Stk4^{tm1.1Rjo}$; $Stk3^{tm1.1Rjo}$, RRID:IMSR_JAX:017635 [17]) mice were obtained from the Jackson Laboratory. *Nr5a1*-cre mice were maintained by crossing *Cre*-positive males with wild-type females (C57BL/6J, RRID:IMSR_JAX:000664) for at least 8 generations. Mice were selectively bred over several generations to obtain $Mst1^{flox/flox}$;$Mst2^{flox/flox}$;*Nr5a1*-cre genotype. From the F3 generation onwards, $Mst1^{flox/flox}$;$Mst2^{flox/flox}$ and $Mst1^{flox/flox}$;$Mst2^{flox/flox}$;*Nr5a1*-cre littermates were used to generate the breeding couples. $Mst1^{flox/flox}$;$Mst2^{flox/flox}$; *Nr5a1*-cre males and females were fertile and both sexes were used as breeders. Experimental and control animals were all littermates and were taken from the F4 generation. Genotype analyses were done on tail biopsies by polymerase chain reaction (PCR) as previously described for Cre [16] or as suggested by the Jackson laboratory for *Mst1/2*.

Histopathology and Immunohistochemistry

Isolated adrenal glands for light microscopy histopathologic analysis were fixed in formalin overnight. Tissues were embedded in paraffin, sectioned (5 µm), and stained with hematoxylin and eosin. Immunohistochemistry was done using VectaStain Elite avidin–biotin complex method kits (Vector Laboratories, Cat# PK-6100, RRID:AB_2336819) or the mouse on mouse elite peroxidase kit (Vector Laboratories, Cat# BMK-2202, RRID:AB_2336833) as directed by the manufacturer. Sections were probed with primary antibodies against cleaved caspase-3 (CAS3) (1:50, Cell signaling, Cat #9661, RRID:AB_234188), Disabled 2, mitogen-responsive phosphoprotein (DAB2) (1:50, BD Biosciences, Cat #610464, RRID:AB_397837), GATA binding protein 4 (GATA4) (1:250, Santa Cruz, Cat# sc-25310, RRID:AB_627667), Ki67 (1:1500, abcam, Cat# ab15580, RRID:AB_443209), NR5A1 (1:100, Cell signaling, Cat# 12800, RRID:AB_2798030), PILR alpha associated neural protein (PIANP)/Liver endothelial differentiated associated protein 1 (1:250, Novus, Cat# NBP1-90541, RRID: AB_11039679), STK3/MST2 (1:100, Cell signaling, Cat# 3952, RRID:AB_2196471), STK4/MST1 (1:1000, Proteintech, Cat# 66663-1-lg, RRID:AB_2882018), Wilms tumor 1 (WT1) (1:300, Cell signaling, Cat# 83535, RRID: AB_2800020), phospho-YAP (1:250, Cell signaling, Cat# 13008, RRID:AB_2650553). Detection was performed using the Vectastain Elite ABC HRP kit, with staining using the 3,3′-diaminobenzidine peroxidase substrate kit (Vector Laboratories).

Adrenocortical Cell Proliferation and Cortex Measurements

Proliferation of adrenocortical cells and accumulation of progenitor-like cells were evaluated using ZEN software (Zen 2012 blue edition; Carl Zeiss Microscopy GmbH 2011). For proliferation, Ki67-positive cells were counted at 400× magnification. Four nonconsecutive sections of whole adrenals from 6-month-old females were analyzed per animal (n = 3) using cell-counting software (ImageJ). The thickness of the spindle-shaped regions of 3 to 4 nonconsecutive sections of whole adrenal from 10-month-old animals was measured per animal (n = 3) by a blind observer using ZEN software.

Hormone Measurements

All assays except for aldosterone were performed by the Center for Research in Reproduction at the Ligand Assay and Analysis Core Laboratory of the University of Virginia. Corticosterone levels were determined by radioimmunoassay (MP Bio, Cat# 07120102, RRID:AB_2783720), luteinizing hormone (LH) levels were determined by in-house 2-site sandwich immunoradiometric assays using monoclonal antibodies against bovine LH (UC Davis, Cat# 518B7, RRID: AB_2756886, provided by Dr. Janet Roser, UC Davis, CA [iodinated tracer antibody]) and against the human LH-beta subunit (Cat #5303, Medix Kauniainen, Finland, RRID: AB_2665513 [capture antibody]). Mouse LH reference prep (AFP5306A; provided by Dr. A.F. Parlow and the National Hormone and Peptide program) was used as standard. Follicle-stimulating hormone (FSH) serum levels were assessed using a mouse/rat multiplex assay (EMD Millipore, Cat# RPTMAG-86K, RRID:AB_2716840) and aldosterone serum levels were determined using the ab136933-Aldosterone enzyme-linked immunosorbent assay kit (Abcam, Cat# ab136933, RRID:AB_2895004). For this, blood samples were collected between 9:30 and 10:00 by cardiac puncture prior to euthanasia. Blood was then allowed to clot at room temperature for 90 minutes and centrifuged at 2000*g* for 15 minutes at room temperature. Serum samples were transferred to polypropylene tubes and stored at

−80 °C until analysis. Intraovarian estradiol levels were determined by enzyme-linked immunosorbent assay (Alpco Diagnostics, Cat# 11-ESTHU-E01, RRID:AB_2756385). For this, ovarian homogenates were obtained by mechanical homogenization in phosphate-buffered saline followed by sonication for 60 seconds. Homogenates were then centrifuged at 10 000*g* for 5 minutes and the supernatants stored at −80 °C until analysis.

Microarray Analyses

Total RNA from adrenal glands of 2-month-old animals was extracted using the Total RNA Mini Kit (FroggaBio) according to the manufacturer's protocol. RNA (n = 3 per group) was submitted to the McGill University and Génome Québec Innovation Centre (Montreal, Quebec, Canada) for RNA quality control and microarray analysis using the Affymetrix Clariom S Mouse assay. Results were analyzed using Transcriptome Analysis Console software (TAC 4.0) (Thermo Fisher Scientific). Thresholds used for *P* value and fold change were .05 and ±2, respectively. Further analyses were performed using the Metascape gene annotation and analysis resource [18]. A protein–protein interaction profile was additionally performed using the string database [19].

Reverse Transcription quantitative PCR

Total RNA from adrenal glands was extracted using the Total RNA Mini Kit (FroggaBio). Total RNA was reverse transcribed using 100 ng of RNA and the SuperScriptVilo™ cDNA synthesis kit (Thermo Fisher scientific). Real-time PCR reactions were run on a CFX96 Touch instrument (Bio-Rad), using Supergreen Advanced qPCR MasterMix (Wisent, St-Bruno, Canada). Each PCR reaction consisted of 7.5 µL of Power SYBR Green PCR Master Mix, 2.3 µL of water, 4 µL of cDNA sample, and 0.6 µL (400 nmol) of gene-specific primers. PCR reactions run without complementary cDNA (water blank) served as negative controls. A common thermal cycling program (3 minutes at 95 °C, 40 cycles of 15 seconds at 95 °C, 30 seconds at 60 °C, and 30 seconds at 72 °C) was used to amplify each transcript. To quantify relative gene expression, the Ct of genes of interest was compared with that of Rpl19, according to the ratio $R = (E^{Ct\ Rpl19}/E^{Ct\ target})$, where E is the amplification efficiency for each primer pair. Rpl19 Ct values did not change significantly between tissues, and Rpl19 was therefore deemed suitable as an internal reference gene. The specific primer sequences used are listed in Table S1 [20].

Statistical Analyses

All statistical analyses were performed with Prism software version 6.0d (GraphPad Software Inc., RRID:SCR_002798). All the data sets were subjected to the *F* test to determine the equality of variances. Statistical significance was determined using the unpaired Student's t-test. Means were considered to be statistically significantly different when $P < .05$. All data are presented as means ± SEM.

Results

MST1 and MST2 are Expressed in the Adrenal Cortex

In order to determine the expression pattern of MST1 and MST2 in the adrenal cortex, immunohistochemistry analyses were performed on adrenal glands from virgin mature female mice. MST1 was mainly detected in the cytoplasm of both the zG and zF cells (Fig. 1A and 1B), as well as in a subpopulation of cells forming the X-zone (Fig. 1A) but was not detected in cells of the capsule surrounding the adrenal cortex (Fig. 1A and 1B). MST1 was also expressed in the nucleus of a subpopulation of chromaffin cells (Fig. 1A). Contrary to MST1, elevated expression of MST2 was detected in the cytoplasm of zG cells but not of zF cells and in cells of the adrenal capsule (Fig. 1C and 1D). Only faint expression of MST2 was detected in cells of the X-zone (Fig. 1C) and in a subpopulation of chromaffin cells (Fig. 1C). The expression pattern of MST1/2 suggest that they might play an important role for the regulation of Hippo signaling in the adrenal cortex as well as for the functions and/or maintenance of the adrenal cortex.

Mst1/2 Ablation Causes Accumulation of Subcapsular Spindle-shaped Cells

To investigate the role of MST1 and MST2 in the adrenal cortex, mice bearing floxed alleles for *Mst1* and *Mst2* were crossed with the *Nr5a1*-cre strain, which targets steroidogenic cells of the adrenal cortex. The double conditional knockout strategy was chosen because MST1 and MST2 have redundant activities and therefore could compensate for the loss of one another [21], especially in the zG where MST1 and MST2 are both expressed. Immunohistochemical analyses of the adrenal gland of $Mst1^{flox/flox}$;$Mst2^{flox/flox}$;*Nr5a1*-cre confirmed the loss of MST1 (Fig. 2B) and MST2 (Fig. 2D) in the adrenal cortex compared with controls (Fig. 2A and 2C, respectively). The maintenance of MST1 and MST2 expression in chromaffin cells (Fig. 2B and 2D) and of MST2 cells in the capsule (Fig. 2D) further confirmed the specificity of the knockout. Surprisingly, MST1 expression was still detected in the X-zone of mutant animals (Fig. 2B), suggesting that recombination was inefficient in the fetal cortex from which it is derived. Consistent with the immunohistochemistry results, RT-qPCR analyses showed 67% and 77% decrease in adrenal *Mst1* and *Mst2* mRNA levels, respectively, in 4-week-old mutant females, and 77% and 80% decrease in *Mst1* and *Mst2* mRNA levels, respectively, in 6-month-old mutant females (Fig. 2E). A similar decrease in *Mst1* and *Mst2* levels was also observed in the adrenal glands of mutant males (Fig. S1 [20]).

Gross morphological level assessment and evaluation of the adrenosomatic index revealed no differences between control and mutant females at 2, 6, and 10 months of age (Fig. S2A [20]). Corticosterone and serum aldosterone levels were also unaltered in 6-month-old females (Fig. S2B and S2C [20]). However, histopathologic analyses revealed the progressive accumulation of basophilic, spindle-shaped cells at the periphery of the cortex (Fig. 3A and 3B). A few spindle-shaped cells were first observed in adrenal cortex of most of the 2-month-old mutant females (3/4), whereas a marked accumulation of these cells was observed in the adrenal cortex of every mutant animal older than 6 months of age (4/4 at 6 months, 5/5 at 10 months) (Fig. 3A and 3B). In control animals, no spindle-shaped cells were observed in 2-month-old females (0/6). Spindle-shaped cells were however found in some aging control animals (1/4 at 6 months, 4/6 at 10 months) (Fig. 3A and 3B), albeit in far fewer numbers than in the mutant mice, with the thickness of the spindle-shaped cell layer being 2.4 times greater in mutant animals than in controls (Fig. 3C). Together, these results suggest that the loss of *Mst1*/2

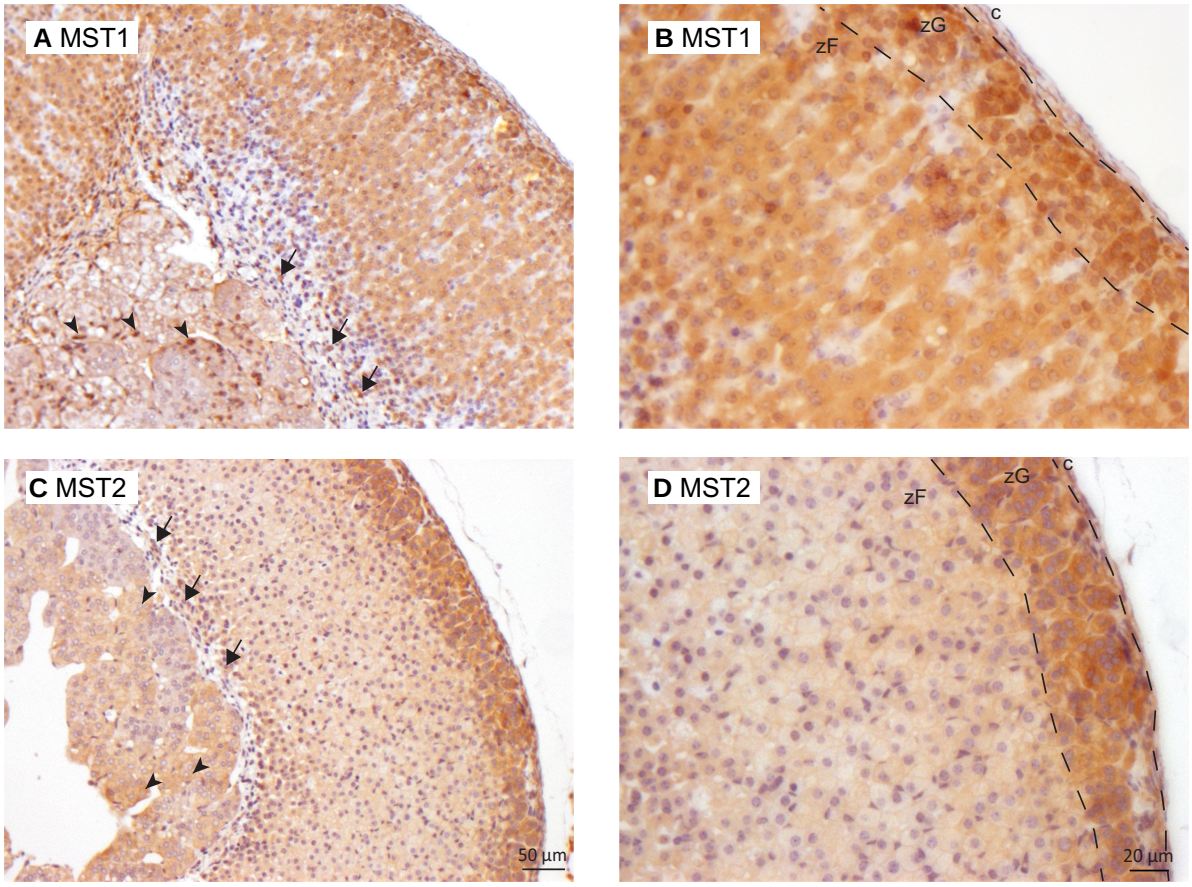

Figure 1. Localization of MST1 and MST2 in the adrenal gland of mice. Immunohistochemical analysis of MST1 (A, B) and MST2 (C). (D) Expression in adrenal glands from 6-month-old virgin female (images B and D are increased magnifications of A and C, respectively). Scale bar in C is valid for A and scale bar in D is valid for B. Arrows, X-zone cells; Arrowheads, chromaffin cells; c, capsule; zF, zona fasciculata; zG, zona glomerulosa.

accelerates the accumulation of the spindle-shaped cells. Interestingly, the expression of MST1 was not detected in the spindle-shaped cells of either the control (Fig. S3A [20]) nor the mutant animals (Fig. S3B [20]). However, MST2 expression was detected in the spindle-shaped cells of the control animals (Fig. S3C [20]) but not in those of *Mst1*$^{flox/flox}$;*Mst2*$^{flox/flox}$;*Nr5a1*-cre animals (Fig. S3D [20]), suggesting that these cells are derived from cells in which the floxed alleles have been recombined (ie, NR5A1, cre-expressing cells). Similar to what was observed in females, the adrenosomatic index did not differ between control and mutant males (Fig. S4A [20]), and a progressive accumulation of spindle-shaped cells was also observed in the adrenal cortex of *Mst1*$^{flox/flox}$;*Mst2*$^{flox/flox}$;*Nr5a1*-cre males (Fig. S4B [20]). For this reason, subsequent experiments were solely performed using female mice.

The accumulation of spindle-shaped cells in the outer adrenal cortex has been observed in older mice and several transgenic mouse models [8, 22–25]. Most interestingly, it has been suggested that these cells are adrenal gonadal primordium (AGP) progenitor-like cells, as they express WT1 and GATA4 (2 genes that are important for the formation of the early adrenal gonadal primordium) but not NR5A1 [25]. To determine if the spindle-shaped cells observed in the adrenal cortex of the *Mst1*$^{flox/flox}$;*Mst2*$^{flox/flox}$;*Nr5a1*-cre animals were also AGP-like progenitor cells, immunohistochemistry for WT1, GATA4, and NR5A1 was performed. As expected, spindle-shaped cells were positive for WT1 (Fig. 4A) and GATA4 (Fig. 4B) and did not express NR5A1 (Fig. 4C).

The accumulation of spindle-shaped cells in the outer adrenal cortex has also been observed in gonadectomized mice, suggesting that sex hormone imbalance is involved in their appearance [26–29]. Taking into account that the *Mst1/2-Nr5a1*-cre–driven conditional deletion can also target hormone-producing cells in the pituitary and the ovary and indirectly affect the adrenal cortex, circulating LH and FSH as well intraovarian estradiol levels were assessed. No differences between LH and FSH serum levels (S5A and S5B [20]) nor intraovarian estradiol levels (Fig. S5C [20]) were observed between control and mutant females. Furthermore, *Mst1*$^{flox/flox}$;*Mst2*$^{flox/flox}$;*Nr5a1*-cre females were fertile. Together, these results suggest that the phenotype observed in the adrenal cortex of *Mst1*$^{flox/flox}$;*Mst2*$^{flox/flox}$;*Nr5a1*-cre animals was not a consequence of sex hormone imbalance.

As it had been previously suggested that the AGP-like progenitor cells originate from the recruitment and proliferation of capsular cells [29], cellular proliferation was evaluated in the adrenal cortex of *Mst1*$^{flox/flox}$;*Mst2*$^{flox/flox}$;*Nr5a1*-cre mice by counting the number of Ki67-expressing cells in the adrenal cortex. No differences in the number of Ki67+ cells were observed between the control and mutant animals (Fig. S6A [20]). Furthermore, Ki67+ cells were randomly distributed in the different zones of the adrenal cortex and the majority of spindle-shaped cells were negative for Ki67

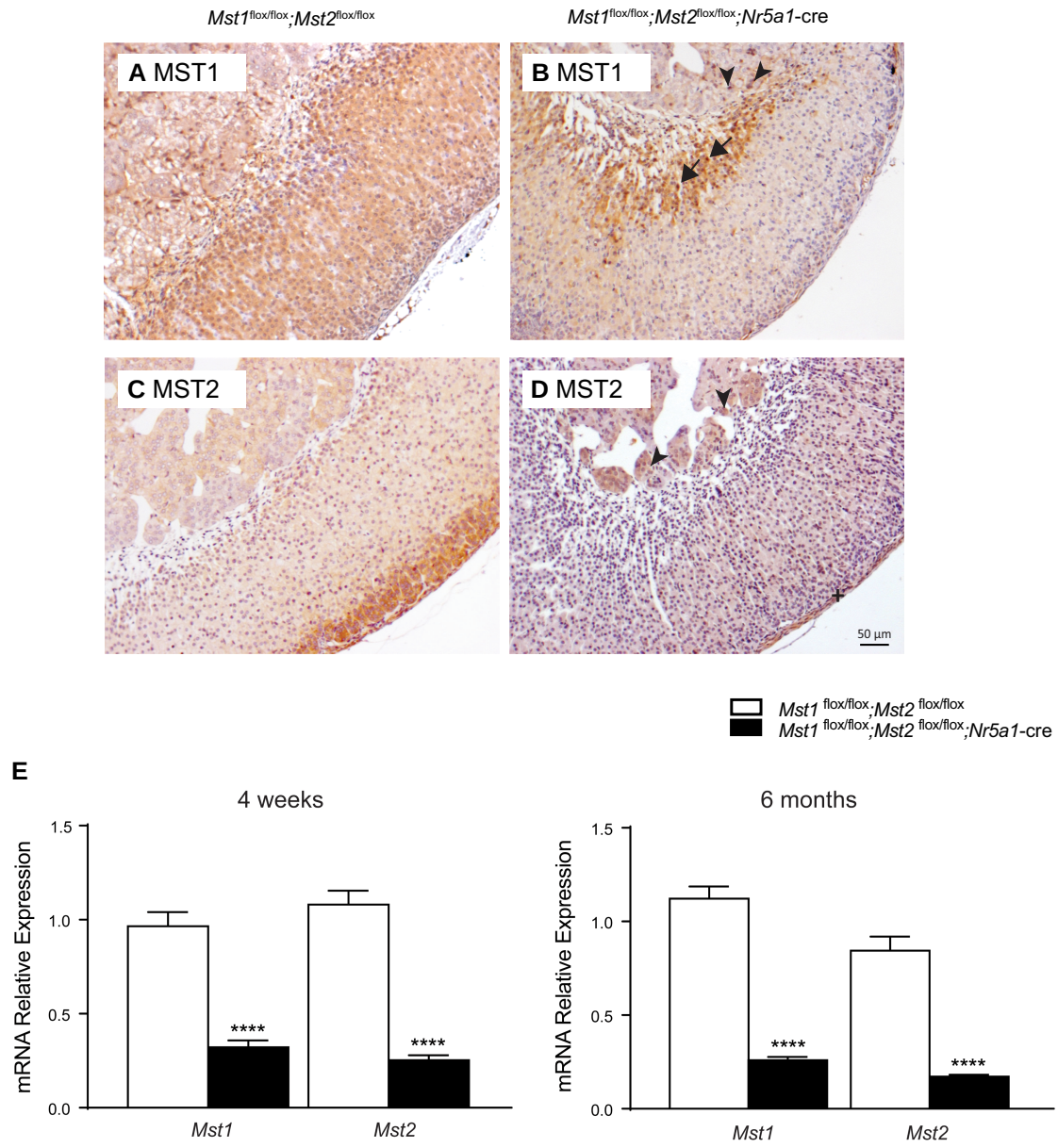

Figure 2. Recombination efficiency in *Mst1*$^{flox/flox}$;*Mst2*$^{flox/flox}$;*Nr5a1*-cre mice. (A, B) Immunohistochemical analysis of MST1 expression in adrenal glands from 6-month-old control (A) and mutant (B) virgin female. (C, D) Immunohistochemical analysis of MST2 expression in adrenal glands from 6-month-old control (C) and mutant (D) virgin female. Scale bar in (D) is valid for all images. Arrows, X-zone cells; arrowheads, chromaffin cells; cross, capsular cells. (E) RT-qPCR analyses of *Lats1* and *Lats2* mRNA levels in the adrenal glands of 4- and 6-month-old virgin female of the indicated genotypes (n = 6 animals/genotype). All data were normalized to the housekeeping gene *Rpl19* and are expressed as means (columns) ± SEM (error bars). Asterisks, significantly different from control (****$P < .0001$).

(Fig. S6B-S6D [20]), suggesting that spindle-shaped cells are not highly proliferative.

Since spindle-shaped cells accumulate in a region where zG cells are normally present, immunohistochemistry for the zG marker DAB2 and for cleaved CAS3 was then respectively performed to determine whether their accumulation affects zG formation or zG cell survival. In 2-month-old control animals, DAB2+ cells were positioned underneath the capsule (Fig. 5A). Proper positioning of DAB2+ cells was also maintained in large regions of the adrenal cortex in 10-month-old control animals (Fig. 5B) and in 2-month-old mutant animals (Fig. 5C). However, in older mutant animals, DAB2+ cells were now mostly located underneath the thick layer of spindle-shaped cells rather than directly underneath the capsule (Fig. 5D). Cleaved-CAS3 labeling showed no differences in apoptosis in the adrenal cortex (including the zG) of mutant animals compared with control, and apoptotic cells were located at the boundary between the medulla and the adrenal cortex in both groups (Fig. S7 [20]). These results are consistent with the lack of change in secreted aldosterone levels in mutant animals and suggest that zG cell identity and function are mostly preserved in *Mst1*$^{flox/flox}$;*Mst2*$^{flox/flox}$;*Nr5a1*-cre animals.

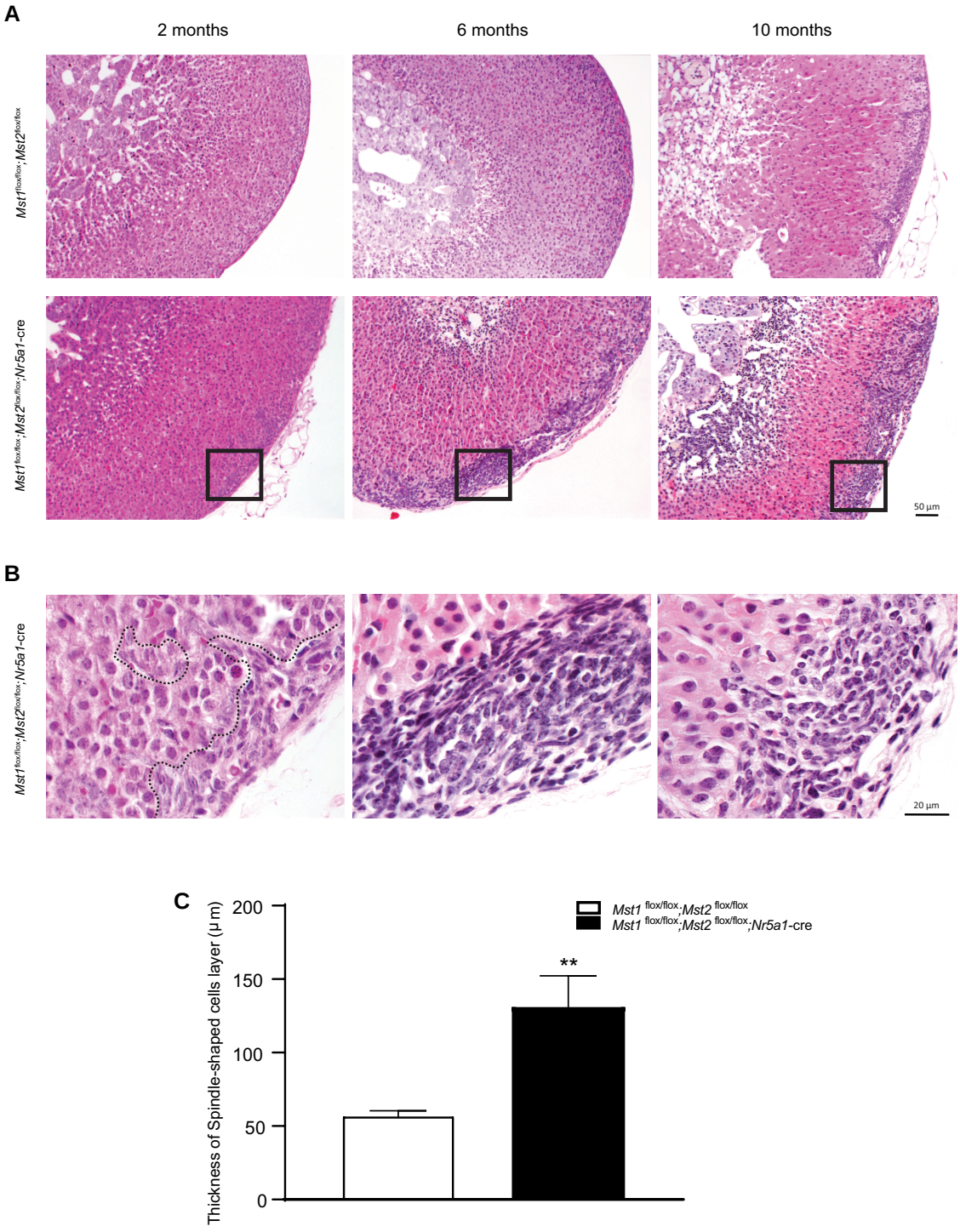

Figure 3. Progressive appearance of spindle-shaped cells in the adrenal cortex of *Mst1*$^{flox/flox}$;*Mst2*$^{flox/flox}$;*Nr5a1*-cre mice. (A) Photomicrographs comparing female adrenal gland histology of *Mst1*$^{flox/flox}$;*Mst2*$^{flox/flox}$;*Nr5a1*-cre with that of *Mst1*$^{flox/flox}$;*Mst2*$^{flox/flox}$ controls at the indicated ages. (B) Photomicrographs of the spindle-shaped cells observed in *Mst1*$^{flox/flox}$;*Mst2*$^{flox/flox}$;*Nr5a1*-cre mice at higher magnification. Scale bar (lower right) is valid for all images. Hematoxylin and eosin stain. Dashed line, delimitation of the spindle-shaped cell population. (C) Measure of the thickness of the zone formed by the spindle-shaped cells in 10-month-old control and mutant animals; 3 to 4 nonconsecutive sections of whole adrenal were measured per animal (n = 4). Data are expressed as means (columns) ± SEM (error bars). Asterisks, significantly different from control (** $P < .01$).

Loss of *Mst1* and *Mst2* Fine-tunes Hippo Signaling Downstream Effector YAP

To determine whether the loss of *Mst1* and *Mst2* leads to the inactivation of Hippo signaling in the adrenal glands of *Mst1*$^{flox/flox}$;*Mst2*$^{flox/flox}$;*Nr5a1*-cre mice, phospho-YAP expression was evaluated by immunohistochemistry in 2- and 10-month-old females. Phospho-YAP was detected in the adrenal cortex of both control and mutant animals (Fig. 6A-6D).

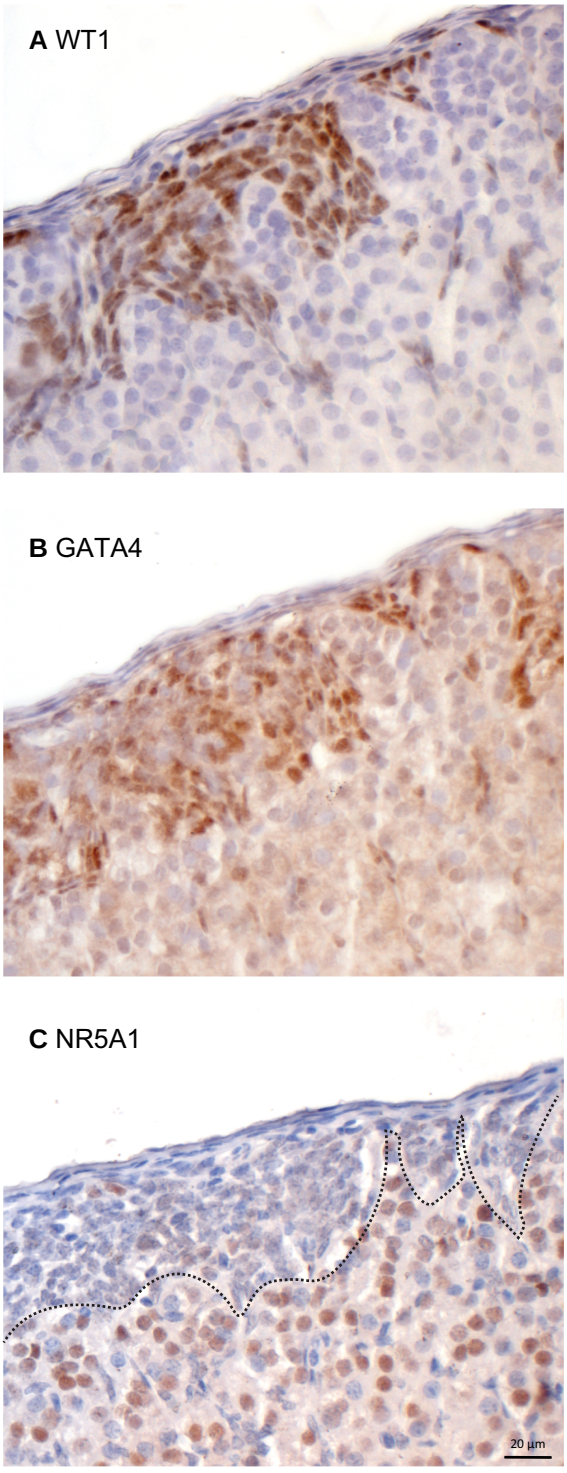

Figure 4. Spindle-shaped cells have characteristics of AGP-like progenitor cells. Immunohistochemical analysis of WT1 (A), GATA4 (B) and NR5A1 (C) expression in adrenal glands from a 2-month-old *Mst1*$^{flox/flox}$;*Mst2*$^{flox/flox}$;*Nr5a1*-cre mice virgin female. Scale bar in (C) is valid for all images.

Interestingly, phospho-YAP was expressed in fewer spindle-shaped cells in mutant animals than in 10-month-old control mice (Fig. 6B-6D). This was consistent with the pattern of expression of MST2 and suggests that Hippo signaling is not active in some of these cells in the mutant animals. These results also suggest that YAP phosphorylation is not essential for spindle-shaped cell formation.

To determine how loss of *Mst1* and *Mst2* affected the transcriptome of the adrenal cortex, adrenal glands from 2-month-old (age at which the phenotypic changes are first observed) *Mst1*$^{flox/flox}$;*Mst2*$^{flox/flox}$;*Nr5a1*-cre and *Mst1*$^{flox/flox}$;*Mst2*$^{flox/flox}$ females were analyzed by microarray (n = 3/genotype). A total of 223 genes were found to be differentially expressed between control and mutant mice by 2-fold or more, of which 143 were upregulated and 80 downregulated (Tables 2 and 3 [20]). The microarray data set was validated by the evaluation of the mRNA levels of selected genes by RT-qPCR (Fig. 7).

Numerous genes known to be YAP transcriptional targets such as *Ajuba* [30–32], aquaporin 1 (*Aqp1*) [33, 34], fibronectin 1 (*Fn1*) [35–38], integrin-binding sialoprotein (*Ibsp*) [39, 40], insulin-like growth factor 1 (*Igf1*) [41], insulin-like growth factor binding protein 2 (*Igfbp2*) [31, 42], matrix metallopeptidase 2 (*Mmp2*) [43], and thrombospondin 1 (*Thbs1*) [44, 45] were upregulated in mutant mice (Table 2 [20]), indicating that YAP transcriptional coregulatory activity is enhanced following *Mst1/2* inactivation. Interestingly, integrin alpha 2 (*Itga2*) [46] and prostaglandin-endoperoxide synthase 2 (*Ptgs2*) [47], 2 genes known to positively regulate YAP activity, were among the most downregulated genes (Table 3 [20]), suggesting the existence of an autoregulatory loop. Together, these results suggest that MST1/2 regulate YAP activity in the adrenal cortex.

Interestingly, *Gata4* was 1 of the genes upregulated following *Mst1/2* deletion confirming that AGP-like progenitor cells were already present in 2-month-old mutant mice. Furthermore, transcription factor 21 (*Tcf21*), which is another marker of the AGP-like progenitor cells [29] was also identified among the upregulated genes again, suggesting the premature presence of these cells in the adrenal gland of mutant animals. To determine if all the upregulated genes were solely expressed in the spindle-shaped cells, the expression of the upregulated gene PIANP was evaluated by immunohistochemistry in the control and the mutant animals. The results showed that in the adrenal cortex of control animals, PIANP was detected in the nucleus of some adrenocortical cells in control animals (Fig. S8A [20]). In *Mst1*$^{flox/flox}$;*Mst2*$^{flox/flox}$;*Nr5a1*-cre animals, PIANP was expressed in the spindle-shaped cells (Fig. S8B [20]) as well as in the nucleus and cytoplasm of a larger proportion of adrenocortical cells (Fig. S8B [20]). Furthermore, a crescent-shaped pattern of perinuclear PIANP staining was observed in a subpopulation of adrenocortical cells in the mutant animals (Fig. S8C [20]), a pattern that was not observed in control animals. PIANP expression suggests that the increase in the expression of some upregulated genes might not be solely attributable to the presence of the spindle-shaped cells.

Unlike the genes that were upregulated in the adrenal cortex of *Mst1*$^{flox/flox}$;*Mst2*$^{flox/flox}$;*Nr5a1*-cre animals, downregulated genes included several genes known to be specifically expressed in the zG or overexpressed in the zG compared with the zF (angiotensin receptor 1b [*Agtr1b*] [48], esophageal cancer related gene 4 [*Ecrg4*] [49], hydroxy-delta-5-steroid dehydrogenase, 3 beta- and steroid delta-isomerase 6 [*Hsd3b6*] [50], nuclear receptor subfamily 0, group B, member 1 [*Nr0b1*] [51, 52], Tescalcin [*Tesc*] [48], and visilin like 1 [*Vsnl1*] [53]; Table 3 [20]). This suggests that MST1/2 contribute to the regulation of zG cell transcriptional activity, despite the lack of clear differences in the abundance of DAB2+

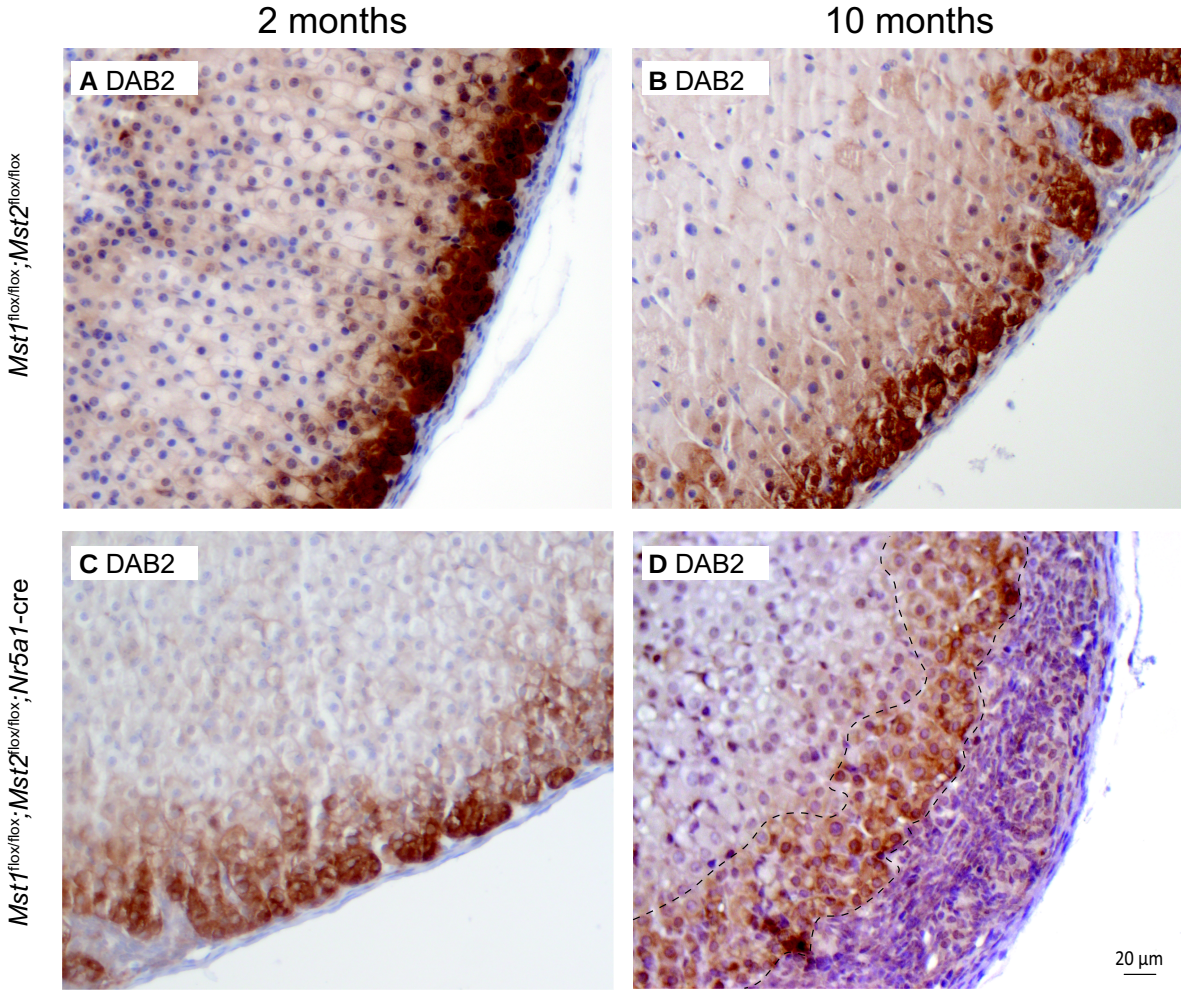

Figure 5. Spindle-shaped cells affect DAB2+ cell positioning. Immunohistochemical analysis of DAB2 in adrenal glands from 2-month-old and 10-month-old *Mst1*$^{flox/flox}$;*Mst2*$^{flox/flox}$ (A, B) and *Mst1*$^{flox/flox}$;*Mst2*$^{flox/flox}$;*Nr5a1*-cre (C, D) virgin females. Scale bar in D is valid for all images. Dashed lines, delimitation of DAB2+ cells.

cells or in aldosterone secretion in *Mst1*$^{flox/flox}$;*Mst2*$^{flox/flox}$;*Nr5a1*-cre mice.

To further study the biological processes affected by the loss of *Mst1/2* in the adrenal cortex of *Mst1*$^{flox/flox}$;*Mst2*$^{flox/flox}$;*Nr5a1*-cre animals, both upregulated and downregulated genes were subjected to gene ontology analysis using Metascape gene annotation and analysis resources. These analyses showed that the main biological processes in which upregulated genes are involved include extracellular matrix organization, regulation of cell adhesion, positive regulation of cell migration, as well as mesenchyme development and response to mechanical stimuli (Fig. S9A [20]). Fewer biological processes were associated with downregulated genes. This list included negative regulation of cell proliferation, regulation of epithelial morphogenesis, and response to steroid hormones (Fig. S9B [20]). Finally, to obtain a better understanding of the relationships between genes affected by the loss of *Mst1/2*, a functional protein association network was generated for regulated genes identified by the microarray (Fig. 8, upregulated genes; Fig. S10, downregulated genes [20]). *Fn1*, *Ibsp*, *Mmp2*, *Thbs1*, and *Igf1* were identified at the center of the network of upregulated genes (Fig. 8), suggesting that they play key roles downstream of MST1/2.

Discussion

In recent years, Hippo signaling has been identified as one of the most important signaling pathways involved in tissue development and homeostasis including in the adrenal cortex. Notably, inactivation of *Yap/Taz* leads to the progressive degeneration of the adrenal cortex [14], whereas the inactivation of *Lats1/2* leads to the transdifferentiation of adrenocortical cells into myofibroblast-like cells and fibrosis [15]. Here, we report that the inactivation of *Mst1* and *Mst2*, the most upstream kinases of the Hippo signaling cascade, leads to the accumulation of subcapsular AGP-like progenitor cells potentially associated with the downregulation of genes specifically expressed in the zG.

The main phenotypic change observed in *Mst1*$^{flox/flox}$;*Mst2*$^{flox/flox}$;*Nr5a1*-cre mice is the premature accumulation of a GATA4+, WT1+ progenitor-like cell population. This cell population is normally observed in the adrenal cortex of aging mice or following gonadectomy [26–29]. Abnormal accumulation of AGP-like progenitor cells has also been observed in several transgenic mouse models [8, 22–25], and it has been suggested that their appearance could be associated with adrenal deficiency, as a supraphysiological accumulation of progenitor cells would be needed to maintain homeostasis

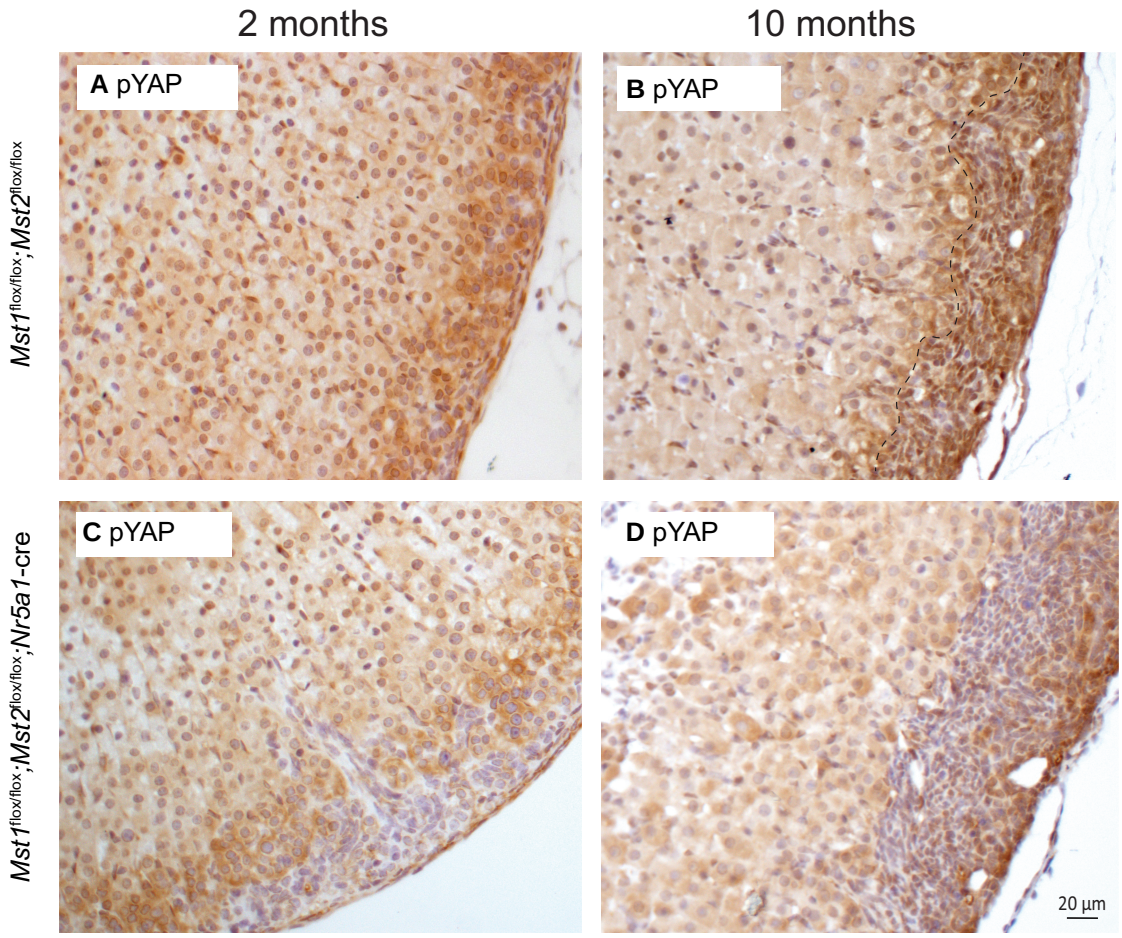

Figure 6. Hippo signaling is inactive in the spindle-shaped cells of mutant animals. Immunohistochemical analysis of phospho-YAP in adrenal glands from 2-month-old and 10-month-old *Mst1*$^{flox/flox}$;*Mst2*$^{flox/flox}$ (A, B) and *Mst1*$^{flox/flox}$;*Mst2*$^{flox/flox}$;*Nr5a1*-cre (C, D) virgin females. Scale bar in D is valid for all images. Dashed line, delimitation of the spindle-shaped cell population.

in this context. Even though the adrenal cortex of mutant animals in the present study appeared phenotypically normal (aside from the accumulation of the spindle-shaped cells) and aldosterone and corticosterone secretion were unchanged, the microarray data showed that the transcriptional activity of zG cells was affected, as the expression of genes known to be specifically expressed or overexpressed in the zG was downregulated following conditional deletion of *Mst1* and *Mst2*. This reduction in transcriptional activity might be associated with a subtle reduction in the activity of zG cells that affects adrenal homeostasis and leads to the premature accumulation of the spindle-shaped cells. On the other hand, it could also suggest that some zG cells dedifferentiate into the AGP-like progenitor cells.

Two developmental origins have been proposed for the AGP-like progenitor cell population. It was originally shown that the spindle-shaped cells arise from WT1+ capsular stem cells [29]. However, recent tracing experiments performed in the *Ezh2*$^{flox/flox}$;*Nr5a1*-cre model suggest that, despite not expressing NR5A1, the spindle-shaped cells observed in this mice model can also originate from the dedifferentiation of NR5A1+ cells [25]. Furthermore, the fact that GATA4 expression preceded WT1 expression in the AGP-like progenitor cells indicates that spindle-shaped cells do not originate from WT1+ cells in the *Ezh2*$^{flox/flox}$;*Nr5a1*-cre model [25]. Though our results do not allow us to conclusively determine the origin of the spindle-shaped cells in the *Mst1*$^{flox/flox}$;*Mst2*$^{flox/flox}$;*Nr5a1*-cre model, the fact that MST2 is not expressed in the spindle-shaped cells of the mutant animals but is maintained in their capsular cells while MST2 is expressed in both the capsular cells and the spindle-shaped cells of the control animals suggests that at least some spindle-shaped cells are derived from NR5A1+ cells present in the adrenal cortex. Nonetheless, tracing experiments marking NR5A1+ cells in the context of the *Mst1*$^{flox/flox}$;*Mst2*$^{flox/flox}$;*Nr5a1*-cre model would be needed to conclusively determine whether the spindle-shaped cells observed in the mutant animals originate solely from the dedifferentiation of steroidogenic adrenocortical cells. Furthermore, NR5A1+ cells in the zG include both the progenitor cells and the aldosterone-producing cells and the transdifferentiation of one or the other cell types could lead to the observed phenotype. Creation of a *Mst1*$^{flox/flox}$;*Mst2*$^{flox/flox}$;*AS*-cre model, in which *Mst1/2* are inactivated specifically in aldosterone-producing cells of the zG without affecting the progenitor cells would be needed to test these nonmutually exclusive hypotheses.

As MST1/2 phosphorylate and activate LATS1/2, it was originally anticipated that the phenotypic changes in the adrenal cortex of the *Mst1*$^{flox/flox}$;*Mst2*$^{flox/flox}$;*Nr5a1*-cre mice would be similar to those observed in *Lats1*$^{flox/flox}$;*Lats2*$^{flox/flox}$;*Nr5a1*-cre animals [12]. Though both models

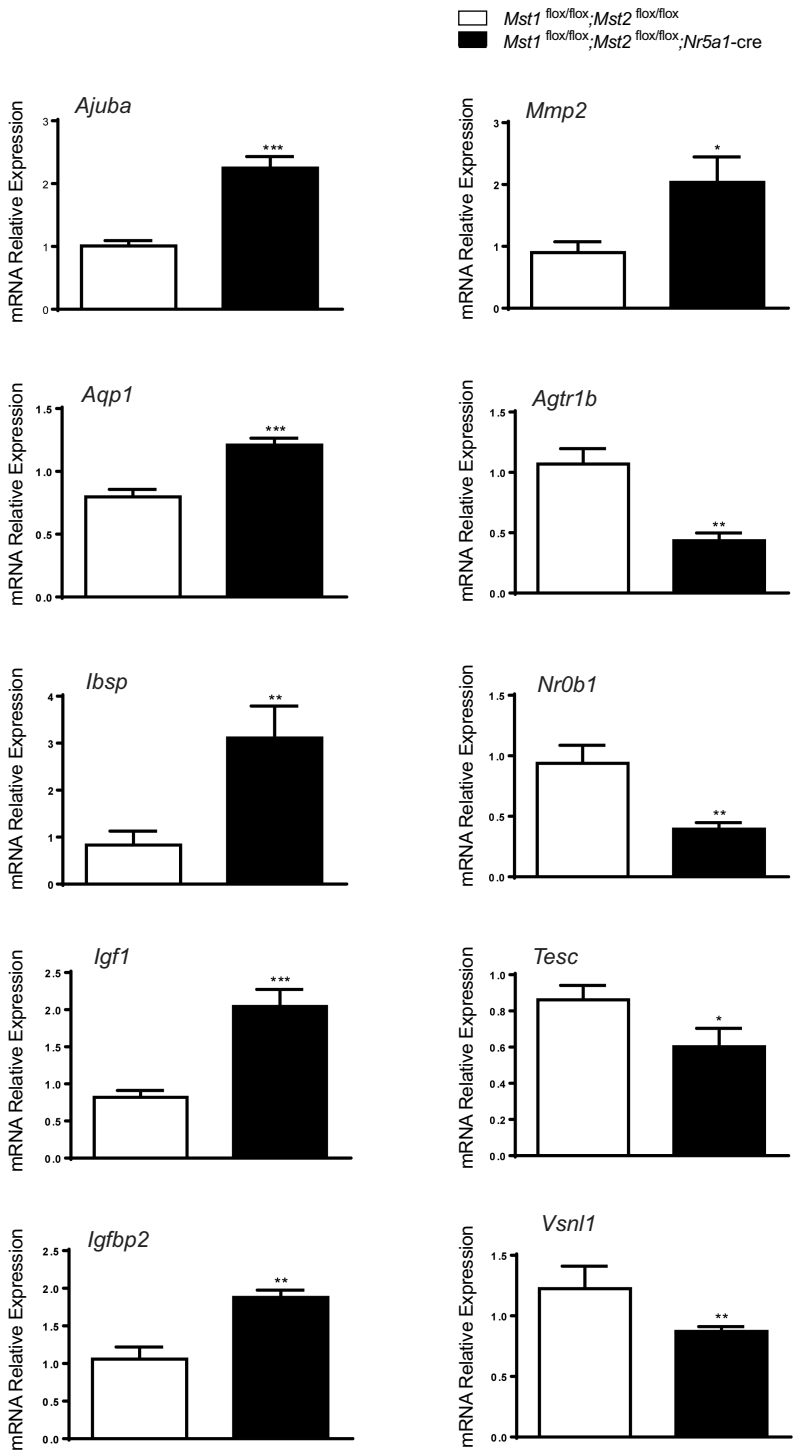

Figure 7. Effects of *Mst1/2* ablation on gene expression. (A) Validation of the microarray data by RT-qPCR analysis (n = 6 for *Mst1*$^{flox/flox}$;*Mst2*$^{flox/flox}$ and n = 6 for *Mst1*$^{flox/flox}$;*Mst2*$^{flox/flox}$;*Nr5a1*-cre 2-month-old virgin females). RT-qPCR data were normalized to the housekeeping gene *Rpl19*. All data are expressed as mean (columns) ± SEM (error bars). Asterisks indicate significant differences from controls (**P* < .05; ***P* < .01; ****P* < .001).

developed spindle-shaped cells in their adrenal cortex, the spindle-shaped cells in the *Lats1*$^{flox/flox}$;*Lats2*$^{flox/flox}$;*Nr5a1*-cre animals were already present by embryonic day e15.5, leading to massive adrenal fibrosis and adrenal failure [15]. It is not known if the spindle-shaped cells observed in both models share some similarities, as high throughput analyses were not performed for the *Lats1*$^{flox/flox}$;*Lats2*$^{flox/flox}$;*Nr5a1*-cre model. However, it is important to note that WT1 expression was only detected in rare adrenocortical cells in *Lats1*$^{flox/flox}$;*Lats2*$^{flox/flox}$;*Nr5a1*-cre animals whereas GATA4 was not detected (Abou Nader et al unpublished data). Another difference between both models is that the phosphorylation of YAP remains elevated in both the zG and the zF in *Mst1*$^{flox/flox}$;*Mst2*$^{flox/flox}$;*Nr5a1*-cre animals, whereas phosphorylation of YAP was drastically reduced in the adrenal cortex of the *Lats1*$^{flox/flox}$;*Lats2*$^{flox/flox}$;*Nr5a1*-cre

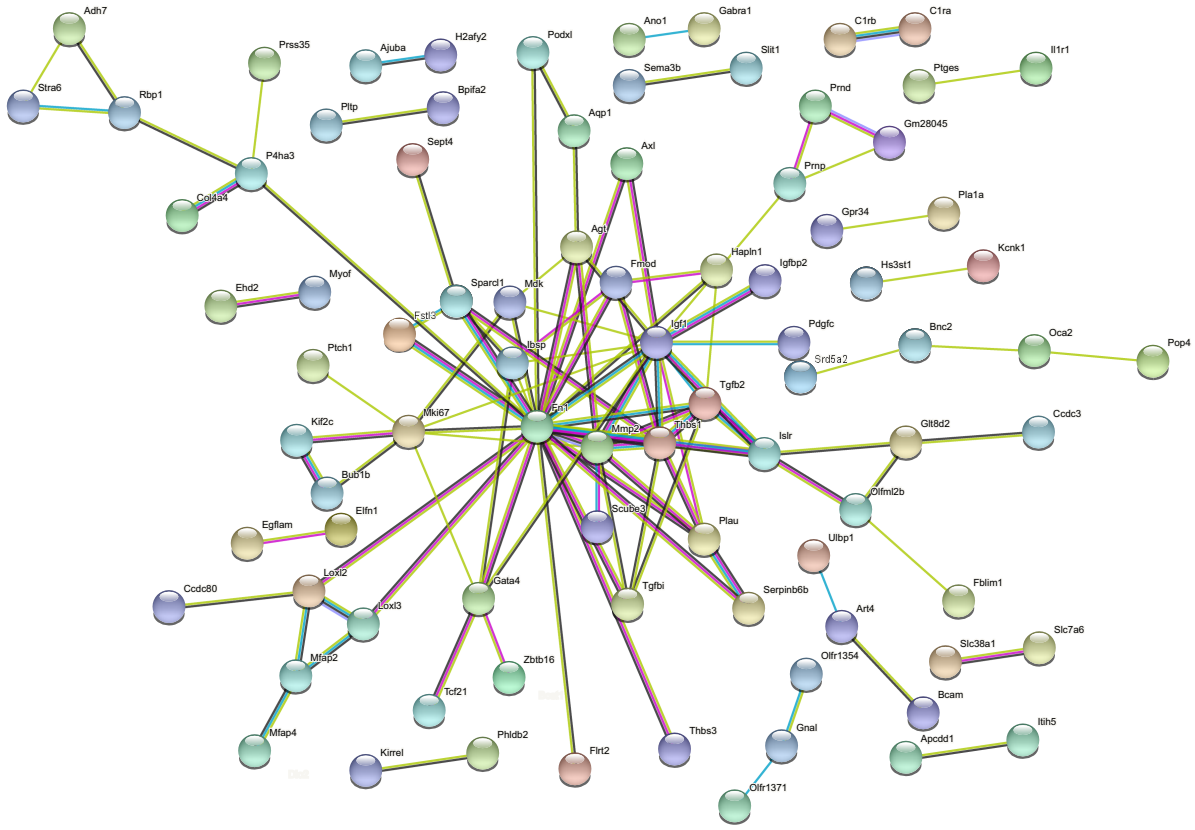

Figure 8. Network of genes with upregulated expression following the loss of *Mst1/2* in the adrenal cortex. Gene network analysis of the upregulated genes in the adrenal cortex of *Mst1*$^{flox/flox}$;*Mst2*$^{flox/flox}$;*Nr5a1*-cre 2-month-old virgin females using the string database. Magenta, experimentally determined interactions; blue, interactions known from curated database; green, predicted interactions, gene neighborhood; violet, protein homology.

animals by e17.5 [15]. This suggests that MST1/2 are not the main kinases that activate LATS1/2 and Hippo signaling in the adrenal cortex. Interestingly, it was shown that the stimulation of GαS-coupled receptors [54, 55] and cyclic adenosine monophosphate/PKA signaling [56, 57] promote Hippo signaling activity and YAP phosphorylation, whereas disruption of GαS–PKA signaling inhibits Hippo signaling [58]. Furthermore, GαS–PKA signaling (which is the main driving force for zF differentiation [7]) can bypass the need for MST1/2 to phosphorylate LATS1/2 [54, 56], suggesting that PKA could directly phosphorylate LATS1/2 in the zF. It was also shown that angiotensin II can regulate Hippo signaling both positively or negatively depending on the context [59–62]; however, MST1/2 were not evaluated in these studies. Aside from PKA signaling, it was shown that mitogen-activated protein kinase kinase kinase kinases (MAP4Ks) can also activate Hippo signaling by directly phosphorylating LATS1/2 in HEK293A cells [63]. This experiment again suggests that MST1/2 could have a limited role in the regulation of Hippo signaling in certain cell types. Nonetheless, the microarray data shown herein demonstrates that MST1/2 fine-tune Hippo signaling, as the expression of known YAP downstream targets is increased in mutant animals.

Even though MST1/2 do not appear to be the main regulators of Hippo signaling in the adrenal cortex, some spindle-shaped cells do not express phospho-YAP in *Mst1*$^{flox/flox}$;*Mst2*$^{flox/flox}$;*Nr5a1*-cre mice, suggesting that MST2 contributes to the regulation of Hippo signaling in these cells. Furthermore, the microarray dataset revealed that the expression of several downstream targets of YAP was upregulated in the adrenal of 2-month-old *Mst1*$^{flox/flox}$;*Mst2*$^{flox/flox}$;*Nr5a1*-cre animals when rare spindle-shaped cells are first observed. Mesenchymal differentiation, cell migration, and matrix organization, all functions known to be regulated by YAP [12, 64, 65], were also among the main biological processes associated with upregulated genes, again suggesting that MST1/2 regulate Hippo signaling in at least a subset of cells of the adrenal cortex.

Finally, among the genes upregulated by MST1/2, 5 of them (*Fn1*, *Ibsp*, *Mmp2*, *Thbs1*, and *Igf1*) were identified at the center of the regulatory network. Interestingly, all 5 of these genes are associated with epithelial to mesenchymal transition [66–70] and are involved in extracellular matrix formation [71–74]. They also have significant roles in tumor formation and/or progression [75–81]. Furthermore, elevated FN1 expression is also associated with the formation of adrenocortical carcinoma [82, 83], and IGF2 (but not IGF1) is overexpressed in most adrenocortical carcinomas [84–86]. *Igf2* overexpression in the adrenal cortex of mutant mice also leads to a phenotype [22] that is similar to that observed in *Mst1*$^{flox/flox}$;*Mst2*$^{flox/flox}$;*Nr5a1*-cre mice, suggesting that IGF signaling might contribute to the phenotype observed in the adrenal gland of *Mst1*$^{flox/flox}$;*Mst2*$^{flox/flox}$;*Nr5a1*-cre animals. Despite the importance of these genes for tumor formation and progression, loss of *Mst1/2* was not sufficient to initiate oncogenic transformation of the adrenal cortex in the *Mst1*$^{flox/flox}$;*Mst2*$^{flox/flox}$;*Nr5a1*-cre model. Nonetheless, homozygous deletions of *MST1* have previously been observed in metastatic adrenocortical carcinoma [87],

suggesting that loss of MST1/2 activity may facilitate tumor progression in the adrenal cortex.

In summary, using a transgenic mouse model inactivating *Mst1/2* specifically in cells of the adrenal cortex, we demonstrated that loss of *Mst1/2* causes the premature accumulation of AGP-like progenitor cells within the adrenal gland by regulating Hippo signaling and expression of genes in zG cells. Further studies will be required to understand the mechanism of action of Hippo signaling throughout the development and maintenance of the adrenal cortex and to better elucidate the interaction between the main kinases of this pathway in this tissue.

Acknowledgments

The authors would like to thank Manon Salvas for technical assistance.

Funding

This work was supported by aDiscovery Grant from the National Sciences and Engineering Reseach Council of Canada (NSERC) (to A.B.). The University of Virginia Center for Research in Reproduction Ligand Assay and Analysis Core is supported by the National Institutes of Health/Eunice Kennedy Shriver National Institute of Child Health and Human Development (Specialized Cooperative Centers Program in Reproduction and Infertility Research) Grant P50-HD28934.

Disclosures

The authors have nothing to disclose.

Data Availability

All data generated during this study are included in this article or in the data repositories listed in reference 26. Microarray data have been deposited in the GEO database under accession number GSE185401 (reviewer token: sbmbyyiczzivnwt).

References

1. Vinson GP. Functional zonation of the adult mammalian adrenal cortex. *Front Neurosci*. 2016;10:238.
2. Grabek A, Dolfi B, Klein B, Jian-Motamedi F, Chaboissier MC, Schedl A. The adult adrenal cortex undergoes rapid tissue renewal in a sex-specific manner. *Cell Stem Cell*. 2019;25(2):290-296.e292.
3. Finco I, Lerario AM, Hammer GD. Sonic hedgehog and WNT signaling promote adrenal gland regeneration in male mice. *Endocrinology*. 2018;159(2):579-596.
4. Pignatti E, Leng S, Yuchi Y, *et al*. Beta-catenin causes adrenal hyperplasia by blocking zonal transdifferentiation. *Cell Rep*. 2020;31(3):107524.
5. Sahut-Barnola I, de Joussineau C, Val P, *et al*. Cushing's syndrome and fetal features resurgence in adrenal cortex-specific Prkar1a knockout mice. *PLoS Genet*. 2010;6(6):e1000980.
6. Drelon C, Berthon A, Sahut-Barnola I, *et al*. PKA inhibits WNT signalling in adrenal cortex zonation and prevents malignant tumour development. *Nat Commun*. 2016;7:12751.
7. Novoselova TV, Hussain M, King PJ, *et al*. MRAP Deficiency impairs adrenal progenitor cell differentiation and gland zonation. *FASEB J*. 2018;32(11):6186-6196.
8. Berthon A, Sahut-Barnola I, Lambert-Langlais S, *et al*. Constitutive beta-catenin activation induces adrenal hyperplasia and promotes adrenal cancer development. *Hum Mol Genet*. 2010;19(8):1561-1576.
9. Dumontet T, Sahut-Barnola I, Septier A, *et al*. PKA signaling drives reticularis differentiation and sexually dimorphic adrenal cortex renewal. *JCI Insight*. 2018;3(2):e98394.
10. Maugeri-Saccà M, De Maria R. The Hippo pathway in normal development and cancer. *Pharmacol Ther*. 2018;186:60-72.
11. Gomez M, Gomez V, Hergovich A. The Hippo pathway in disease and therapy: cancer and beyond. *Clin Transl Med*. 2014;3:22.
12. Piccolo S, Dupont S, Cordenonsi M. The biology of YAP/TAZ: Hippo signaling and beyond. *Physiol Rev*. 2014;94(4):1287-1312.
13. Varelas X. The Hippo pathway effectors TAZ and YAP in development, homeostasis and disease. *Development*. 2014;141(8):1614-1626.
14. Levasseur A, St-Jean G, Paquet M, Boerboom D, Boyer A. Targeted disruption of YAP and TAZ impairs the maintenance of the adrenal cortex. *Endocrinology*. 2017;158(11):3738-3753.
15. Ménard A, Abou Nader N, Levasseur A, *et al*. Targeted disruption of Lats1 and Lats2 in mice impairs adrenal cortex development and alters adrenocortical cell fate. *Endocrinology*. 2020;161(6):bqaa052.
16. Dhillon H, Zigman JM, Ye C, *et al*. Leptin directly activates SF1 neurons in the VMH, and this action by leptin is required for normal body-weight homeostasis. *Neuron*. 2006;49(2):191-203.
17. Lu L, Li Y, Kim SM, *et al*. Hippo signaling is a potent in vivo growth and tumor suppressor pathway in the mammalian liver. *Proc Natl Acad Sci U S A*. 2010;107(4):1437-1442.
18. Zhou Y, Zhou B, Pache L, *et al*. Metascape provides a biologist-oriented resource for the analysis of systems-level datasets. *Nat Commun*. 2019;10(1):1523.
19. Szklarczyk D, Gable AL, Lyon D, *et al*. STRING V11: protein-protein association networks with increased coverage, supporting functional discovery in genome-wide experimental datasets. *Nucleic Acids Res*. 2019;47(D1):D607-D613.
20. Abou Nader N, Blais E, St-Jean G, Boerboom D, Zamberlam G, Boyer A. Supplemental data for "Effect of inactivation of Mst1 and Mst2 in the mouse adrenal cortex", Borealis, V1. http://doi.org/10.5683/SP3/A58HJT.
21. Galan JA, Avruch J. MST1/MST2 protein kinases: regulation and physiologic roles. *Biochemistry*. 2016;55(39):5507-5519.
22. Drelon C, Berthon A, Ragazzon B, *et al*. Analysis of the role of Igf2 in adrenal tumour development in transgenic mouse models. *PLoS One*. 2012;7(8):e44171.
23. Chrusciel M, Vuorenoja S, Mohanty B, *et al*. Transgenic GATA-4 expression induces adrenocortical tumorigenesis in C57Bl/6 mice. *J Cell Sci*. 2013;126(Pt 8):1845-1857.
24. Pihlajoki M, Gretzinger E, Cochran R, *et al*. Conditional mutagenesis of Gata6 in SF1-positive cells causes gonadal-like differentiation in the adrenal cortex of mice. *Endocrinology*. 2013;154(5):1754-1767.
25. Mathieu M, Drelon C, Rodriguez S, *et al*. Steroidogenic differentiation and PKA signaling are programmed by histone methyltransferase EZH2 in the adrenal cortex. *Proc Natl Acad Sci U S A*. 2018;115(52):E12265-E12274.
26. Bielinska M, Kiiveri S, Parviainen H, Mannisto S, Heikinheimo M, Wilson DB. Gonadectomy-induced adrenocortical neoplasia in the domestic ferret (Mustela putorius furo) and laboratory mouse. *Vet Pathol*. 2006;43(2):97-117.
27. Krachulec J, Vetter M, Schrade A, *et al*. GATA4 is a critical regulator of gonadectomy-induced adrenocortical tumorigenesis in mice. *Endocrinology*. 2012;153(6):2599-2611.
28. Dörner J, Martinez Rodriguez V, Ziegler R, *et al*. GLI1(+) progenitor cells in the adrenal capsule of the adult mouse give rise to heterotopic gonadal-like tissue. *Mol Cell Endocrinol*. 2017;441:164-175.
29. Bandiera R, Vidal VP, Motamedi FJ, *et al*. WT1 Maintains adrenal-gonadal primordium identity and marks a population of AGP-like progenitors within the adrenal gland. *Dev Cell*. 2013;27(1):5-18.

30. Zanconato F, Forcato M, Battilana G, *et al*. Genome-wide association between YAP/TAZ/TEAD and AP-1 at enhancers drives oncogenic growth. *Nat Cell Biol*. 2015;17(9):1218-1227.
31. Rozengurt E, Sinnett-Smith J, Eibl G. Yes-associated protein (YAP) in pancreatic cancer: at the epicenter of a targetable signaling network associated with patient survival. *Signal Transduct Target Ther*. 2018;3(1):11.
32. Lange AW, Sridharan A, Xu Y, Stripp BR, Perl A-K, Whitsett JA. Hippo/Yap signaling controls epithelial progenitor cell proliferation and differentiation in the embryonic and adult lung. *J Mol Cell Biol*. 2015;7(1):35-47.
33. Xu J, Li P-X, Wu J, *et al*. Involvement of the Hippo pathway in regeneration and fibrogenesis after ischaemic acute kidney injury: YAP is the key effector. *Clin Sci*. 2016;130(5):349-363.
34. Nishio M, Sugimachi K, Goto H, *et al*. Dysregulated YAP1/TAZ and TGF-β signaling mediate hepatocarcinogenesis in Mob1a/1b-deficient mice. *Proc Natl Acad Sci U S A*. 2016;113(1):E71-E80.
35. Liu F, Lagares D, Choi KM, *et al*. Mechanosignaling through YAP and TAZ drives fibroblast activation and fibrosis. *Am J Physiol-Lung Cell Mol Physiol*. 2015;308(4):L344-L357.
36. Bhat KP, Salazar KL, Balasubramaniyan V, *et al*. The transcriptional coactivator TAZ regulates mesenchymal differentiation in malignant glioma. *Genes Dev*. 2011;25(24):2594-2609.
37. Chen Y, Zhao X, Sun J, *et al*. YAP1/Twist promotes fibroblast activation and lung fibrosis that conferred by miR-15a loss in IPF. *Cell Death Differ*. 2019;26(9):1832-1844.
38. Mia MM, Cibi DM, Ghani SABA, *et al*. Loss of YAP/TAZ in cardiac fibroblasts attenuates adverse remodelling and improves cardiac function. *Cardiovasc Res*. 2022;118(7):1785-1804.
39. Tao S-C, Gao Y-S, Zhu H-Y, *et al*. Decreased extracellular pH inhibits osteogenesis through proton-sensing GPR4-mediated suppression of yes-associated protein. *Sci Rep*. 2016;6:26835-26835.
40. Goodwin AF, Chen CP, Vo NT, Bush JO, Klein OD. YAP/TAZ regulate elevation and bone formation of the mouse secondary palate. *J Dental Res*. 2020;99(12):1387-1396.
41. Xin M, Kim Y, Sutherland LB, *et al*. Regulation of insulin-like growth factor signaling by Yap governs cardiomyocyte proliferation and embryonic heart size. *Sci Signal*. 2011;4(196):ra70.
42. Wang J, Liu S, Heallen T, Martin JF. The Hippo pathway in the heart: pivotal roles in development, disease, and regeneration. *Nat Rev Cardiol*. 2018;15(11):672-684.
43. Pan Z, Tian Y, Zhang B, *et al*. YAP signaling in gastric cancer-derived mesenchymal stem cells is critical for its promoting role in cancer progression. *Int J Oncol*. 2017;51(4):1055-1066.
44. Shen J, Cao B, Wang Y, *et al*. Hippo component YAP promotes focal adhesion and tumour aggressiveness via transcriptionally activating THBS1/FAK signalling in breast cancer. *J Exp Clin Cancer Res*. 2018;37(1):175.
45. Schütte U, Bisht S, Heukamp LC, *et al*. Hippo signaling mediates proliferation, invasiveness, and metastatic potential of clear cell renal cell carcinoma. *Transl Oncol*. 2014;7(2):309-321.
46. Wong K-F, Liu AM, Hong W, Xu Z, Luk JM. Integrin α2β1 inhibits MST1 kinase phosphorylation and activates yes-associated protein oncogenic signaling in hepatocellular carcinoma. *Oncotarget*. 2016;7(47):77683-77695.
47. Xu G, Wang Y, Li W, *et al*. COX-2 forms regulatory loop with YAP to promote proliferation and tumorigenesis of hepatocellular carcinoma cells. *Neoplasia*. 2018;20(4):324-334.
48. Nishimoto K, Rigsby CS, Wang T, *et al*. Transcriptome analysis reveals differentially expressed transcripts in rat adrenal zona glomerulosa and zona fasciculata. *Endocrinology*. 2012;153(4):1755-1763.
49. Porzionato A, Rucinski M, Macchi V, Sarasin G, Malendowicz LK, De Caro R. ECRG4 expression in normal rat tissues: expression study and literature review. *Eur J Histochem*. 2015;59(2):2458-2458.
50. Yamamura K, Doi M, Hayashi H, *et al*. Immunolocalization of murine type VI 3β-hydroxysteroid dehydrogenase in the adrenal gland, testis, skin, and placenta. *Mol Cell Endocrinol*. 2014;382(1):131-138.
51. Kawabe K, Shikayama T, Tsuboi H, *et al*. Dax-1 as one of the target genes of Ad4BP/SF-1. *Mol Endocrinol*. 1999;13(8):1267-1284.
52. Mukai T, Kusaka M, Kawabe K, *et al*. Sexually dimorphic expression of Dax-1 in the adrenal cortex. *Genes Cells*. 2002;7(7):717-729.
53. Trejter M, Hochol A, Tyczewska M, *et al*. Visinin-like peptide 1 in adrenal gland of the rat. Gene expression and its hormonal control. *Peptides*. 2015;63:22-29.
54. Yu F-X, Zhao B, Panupinthu N, *et al*. Regulation of the hippo-YAP pathway by G-protein-coupled receptor signaling. *Cell*. 2012;150(4):780-791.
55. Deng Y, Wu LMN, Bai S, *et al*. A reciprocal regulatory loop between TAZ/YAP and G-protein gαs regulates Schwann cell proliferation and myelination. *Nat Commun*. 2017;8:15161-15161.
56. Yu F-X, Zhang Y, Park HW, *et al*. Protein kinase A activates the hippo pathway to modulate cell proliferation and differentiation. *Genes Dev*. 2013;27(11):1223-1232.
57. Zhang L, Noguchi YT, Nakayama H, *et al*. The CalcR-PKA-Yap1 axis is critical for maintaining quiescence in muscle stem cells. *Cell Rep*. 2019;29(8):2154-2163.e2155.
58. Iglesias-Bartolome R, Torres D, Marone R, *et al*. Inactivation of a Gα(s)-PKA tumour suppressor pathway in skin stem cells initiates basal-cell carcinogenesis. *Nat Cell Biol*. 2015;17(6):793-803.
59. Lin M, Yuan W, Su Z, *et al*. Yes-associated protein mediates angiotensin II-induced vascular smooth muscle cell phenotypic modulation and hypertensive vascular remodelling. *Cell Prolif*. 2018;51(6):e12517.
60. Jin B, Zhu J, Shi H-M, Wen Z-C, Wu B-W. YAP activation promotes the transdifferentiation of cardiac fibroblasts to myofibroblasts in matrix remodeling of dilated cardiomyopathy. *Braz J Med Biol Res*. 2018;52(1):e7914-e7914.
61. Wennmann DO, Vollenbröker B, Eckart AK, *et al*. The hippo pathway is controlled by angiotensin II signaling and its reactivation induces apoptosis in podocytes. *Cell Death Dis*. 2014;5(11):e1519-e1519.
62. Wu P, Liu Z, Zhao T, *et al*. Lovastatin attenuates angiotensin II induced cardiovascular fibrosis through the suppression of YAP/TAZ signaling. *Biochem Biophys Res Commun*. 2019;512(4):736-741.
63. Meng Z, Moroishi T, Mottier-Pavie V, *et al*. MAP4K family kinases act in parallel to MST1/2 to activate LATS1/2 in the Hippo pathway. *Nat Commun*. 2015;6:8357.
64. Kim C-L, Choi S-H, Mo J-S. Role of the hippo pathway in fibrosis and cancer. *Cells*. 2019;8(5):468.
65. Elbediwy A, Vincent-Mistiaen ZI, Thompson BJ. YAP And TAZ in epithelial stem cells: a sensor for cell polarity, mechanical forces and tissue damage. *Bioessays*. 2016;38(7):644-653.
66. Aiello NM, Kang Y. Context-dependent EMT programs in cancer metastasis. *J Exp Med*. 2019;216(5):1016-1026.
67. Wang M, Liu B, Li D, *et al*. Upregulation of IBSP expression predicts poor prognosis in patients with esophageal squamous cell carcinoma. *Front Oncol*. 2019;9:1117-1117.
68. Liu X, Xu D, Liu Z, *et al*. THBS1 facilitates colorectal liver metastasis through enhancing epithelial-mesenchymal transition. *Clin Transl Oncol*. 2020;22(10):1730-1740.
69. Leal-Orta E, Ramirez-Ricardo J, Garcia-Hernandez A, Cortes-Reynosa P, Salazar EP. Extracellular vesicles from MDA-MB-231 breast cancer cells stimulated with insulin-like growth factor 1 mediate an epithelial-mesenchymal transition process in MCF10A mammary epithelial cells. *J Cell Commun Signal*. 2021. Doi: 10.1007/s12079-021-00638-y
70. Zhu Y, Yan L, Zhu W, Song X, Yang G, Wang S. MMP2/3 Promote the growth and migration of laryngeal squamous cell carcinoma via PI3K/akt-NF-κB-mediated epithelial-mesenchymal transformation. *J Cell Physiol*. 2019. Doi: 10.1002/jcp.28242
71. Theocharis AD, Skandalis SS, Gialeli C, Karamanos NK. Extracellular matrix structure. *Adv Drug Deliv Rev*. 2016;97:4-27.

72. Ganss B, Kim RH, Sodek J. Bone sialoprotein. *Crit Rev Oral Biol Med*. 1999;10(1):79-98.
73. Yamashiro Y, Thang BQ, Ramirez K, *et al*. Matrix mechanotransduction mediated by thrombospondin-1/integrin/YAP in the vascular remodeling. *Proc Natl Acad Sci U S A*. 2020;117(18):9896-9905.
74. Monzo HJ, Park TI, Dieriks BV, *et al*. Insulin and IGF1 modulate turnover of polysialylated neural cell adhesion molecule (PSA-NCAM) in a process involving specific extracellular matrix components. *J Neurochem*. 2013;126(6):758-770.
75. Detmar M. Tumor angiogenesis. *J Invest Dermatol Symp Proc*. 2000;5(1):20-23.
76. Jezierska A, Motyl T. Matrix metalloproteinase-2 involvement in breast cancer progression: a mini-review. *Med Sci Monit*. 2009;15(2):Ra32-40.
77. Qiao P, Lu ZR. Fibronectin in the tumor microenvironment. *Adv Exp Med Biol*. 2020;1245:85-96.
78. Chen Y, Qin Y, Dai M, *et al*. IBSP, a potential recurrence biomarker, promotes the progression of colorectal cancer via Fyn/β-catenin signaling pathway. *Cancer Med*. 2021;10(12):4030-4045.
79. Ge J, Chen Z, Huang J, Yuan W, Den Z, Chen Z. Silencing insulin-like growth factor-1 receptor expression inhibits gastric cancer cell proliferation and invasion. *Mol Med Rep*. 2015;11(1):633-638.
80. Zhang Y, Moerkens M, Ramaiahgari S, *et al*. Elevated insulin-like growth factor 1 receptor signaling induces antiestrogen resistance through the MAPK/ERK and PI3K/akt signaling routes. *Breast Cancer Res*. 2011;13(3):R52.
81. Kang HJ, Yi YW, Kim HJ, Hong YB, Seong YS, Bae I. BRCA1 Negatively regulates IGF-1 expression through an estrogen-responsive element-like site. *Cell Death Dis*. 2012;3(6):e336.
82. Bulzico D, de Faria PAS, Maia CB, *et al*. Is there a role for epithelial-mesenchymal transition in adrenocortical tumors? *Endocrine*. 2017; 58(2):276-288.
83. Moon SJ, Kim JH, Kong SH, Shin CS. Protein expression of cyclin B1, transferrin receptor, and fibronectin is correlated with the prognosis of adrenal cortical carcinoma. *Endocrinol Metab (Seoul)*. 2020;35(1):132-141.
84. Ilvesmäki V, Kahri AI, Miettinen PJ, Voutilainen R. Insulin-like growth factors (IGFs) and their receptors in adrenal tumors: high IGF-II expression in functional adrenocortical carcinomas. *J Clin Endocrinol Metab*. 1993;77(3):852-858.
85. De Fraipont F, Le Moigne G, Defaye G, *et al*. Transcription profiling of benign and malignant adrenal tumors by cDNA macro-array analysis. *Endocr Res*. 2002;28(4):785-786.
86. Erickson LA, Jin L, Sebo TJ, *et al*. Pathologic features and expression of insulin-like growth factor-2 in adrenocortical neoplasms. *Endocr Pathol*. 2001;12(4):429-435.
87. Gara SK, Lack J, Zhang L, Harris E, Cam M, Kebebew E. Metastatic adrenocortical carcinoma displays higher mutation rate and tumor heterogeneity than primary tumors. *Nat Commun*. 2018;9(1):4172.